

Conformational Preferences of *N*-Acetyl-L-leucine-*N'*-methylamide. Gas-Phase and Solution Calculations on the Model Dipeptide

Marcelo F. Masman,[†] Sándor Lovas,[‡] Richard F. Murphy,[‡] Ricardo D. Enriz,[†] and Ana M. Rodríguez^{*,†}

Departamento de Química, Universidad Nacional de San Luis, Chacabuco 917, 5700 San Luis, Argentina, and Department of Biomedical Sciences, Creighton University, 2500 California Plaza, Omaha, Nebraska 68178

Received: March 1, 2007; In Final Form: June 12, 2007

A DFT study of *N*-acetyl-L-leucine-*N'*-methylamide conformers in the gas phase and in solution was carried out. The theoretical computational analysis revealed 43 different conformations at the B3LYP/6-31G(d) level of theory in the gas phase. In addition, the effects of three solvents (water, acetonitrile, and chloroform) were included in the calculations using the isodensity polarizable continuum model (IPCM) and the Poisson–Boltzmann self-consistent reaction field (PB-SCRF) method. The stability order of the different conformers in solution has been analyzed. The theoretical results were compared with some experimental data (X-ray, IR, and NMR).

1. Introduction

Conformational preferences of single amino acid residues in the context of a polypeptide sequence are of great interest^{1–7} because folding pathways of protein molecules must be primarily restricted by the total conformational space determined by the individual amino acid residues.

A fundamental question that has not been satisfactorily answered yet is how side chains and backbones interact in peptides. Side-chain folding is not only interesting but also important because side-chain orientation can influence backbone folding via side-chain/backbone interaction. In fact, the analysis of the phenomenon of side-chain folding requires relatively long aliphatic side chains, and there are only a handful of amino acids that fulfill this requirement. The isomeric amino acids leucine and isoleucine have branched and strongly hydrophobic four-carbon side chains, with the only difference in the branching position. Isoleucine possesses a β -branched side chain and leucine, a γ -branched side chain. Both residues have powerful capacities for inducing ordered secondary structures in a polypeptide chain. Leucine is considered to be the strongest α -helix-forming residue.^{8–10} However, the analysis of the leucine residue distribution between helical and nonhelical regions in globular proteins also gives no real arguments to ascribe special helix-forming properties to leucine.¹¹ On the other hand, isoleucine, due to its bulkiness at the β -position, strongly favors the β -conformation.^{12–14} As both helix and β -conformations are stabilized by hydrophobic contributions,^{15–18} these strongly hydrophobic residues are excellent candidates for participation in the nucleation of these secondary structures.

Concerning isoleucine, we reported an exhaustive conformational and electronic study of *N*-acetyl-L-isoleucine-*N*-methylamide in the gas phase and in solution showing the influence of its nonpolar side chain on the conformational preferences.¹⁹ Density functional theory (DFT) calculations predicted the γ_L (C₇^{eq}) and β_L (C₅) forms as the highly preferred conformations

in the gas phase. In contrast, the β_L and particularly the α_L forms were significantly favored by effects of three different solvents. The results obtained for the right-handed helix (α_L) conformations of isoleucine compared with those attained previously for glutamate,²⁰ glutamine,²¹ and aspartic acid²² offered new insight into the influence of charged and noncharged (polar or nonpolar) side chains on the conformational preferences. Thus, it was demonstrated that the insertion of a nonpolar side chain into a peptide structure is conformationally relevant, producing significant structural changes.¹⁹

In light of the above background, we here focus on the amino acid L-leucine because this amino acid has, as well as isoleucine, a long enough nonpolar side chain and has been recognized as an important residue that participates in the inter- and intramolecular hydrophobic interactions based on its lipophilic side chain in polypeptides.^{23–26} Therefore, it is of interest to predict by theoretical methods the structure and relative stability of leucine and, more important, to prove that these theoretical methods serve as a reliable tool in the modeling of biological systems and processes.

The present paper is the first in which the full conformational space of *N*-acetyl-L-leucine-*N'*-methylamide (**I**, Figure 1) has been calculated at the RHF/3-21G and B3LYP/6-31G(d) levels of theory in the gas phase and also in various solvents by applying the isodensity polarizable continuum model (IPCM)²⁷ and the Poisson–Boltzmann self-consistent reaction field (PB-SCRF) method.^{28,29} Three dielectric constants of media, i.e., 4.90, 36.64, and 78.39 (corresponding to chloroform, acetonitrile, and water, respectively), have been selected. Our results have been compared with experimental data. The electron correlation and the solvent effects on the conformational preferences of leucine dipeptide have been studied in detail.

2. Methods

2.1. Nomenclature and Abbreviations. For any given peptide with two optimizable dihedral angles about the peptide bond, ϕ and ψ , the laws of multidimensional conformational analysis (MDCA)^{30–32} predict nine possible backbone (BB)

* Corresponding author. E-mail: amrodri@unsl.edu.ar.

[†] Universidad Nacional de San Luis.

[‡] University of Creighton.

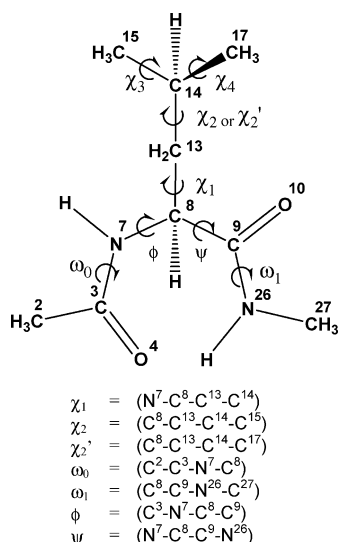


Figure 1. Numbering system employed for $\text{CH}_3\text{CO-Leu-NHCH}_3$ with definition of backbone and side-chain dihedral angles.

conformations. These conformations are often depicted on a Ramachandran map and labeled as α_D (α_{left}), ϵ_D , γ_D (C_7^{ax}), δ_L (β_2), β_L (C_5), δ_D (α'), γ_L (C_7^{eq}), ϵ_L (PPII), and α_L (α_{right}) (Figure 2a). IUPAC–IUB³³ rules recommend the use of $0^\circ \rightarrow +180^\circ$ for clockwise rotation and $0^\circ \rightarrow -180^\circ$ for counterclockwise rotation ($-180^\circ \leq \phi \leq 180^\circ$ and $-180^\circ \leq \psi \leq 180^\circ$).

In Leu, there are four additional dihedral angles of interest in the side chain (SC): χ_1 , χ_2 , χ_3 , and χ_4 (Figure 1). For SC rotation, this implies the following range: $-180^\circ \leq \chi_1 \leq 180^\circ$, $-180^\circ \leq \chi_2 \leq 180^\circ$, $-180^\circ \leq \chi_3 \leq 180^\circ$, and $-180^\circ \leq \chi_4 \leq 180^\circ$. Like the BB dihedrals, each SC dihedral can assume three possible conformations, gauche+ ($g^+ \cong 60^\circ$), anti ($a \cong 180^\circ$), and gauche- ($g^- \cong -60^\circ$), leading to $3 \times 3 = 9$ possible SC conformations (Figure 2b).

2.2. Molecular Computations of Structures and Energies.

All gas-phase computations were carried out using the Gaussian 03 program package (G03).³⁴ Each structure was initially optimized using the ab initio³⁵ restricted Hartree–Fock (RHF)³⁶ method with the split valence 3-21G basis set.^{37–39} The RHF/3-21G geometry optimized structural parameters were then used as the input in a subsequent theoretical refinement step with the inclusion of electron correlation effects at the B3LYP/6-31G(d) level of theory to obtain more reliable geometry and stability data. Here, B3LYP⁴⁰ denotes the combination of Becke's three-parameter exchange functional with the Lee–Yang–Parr (LYP)⁴¹ correlation functional and also employs the mathematically more complete 6-31G(d) basis set. Total energies are given in hartrees, and the relative energies are given in kilocalories per mole (with the conversion factor 1 hartree = 627.5095 kcal·mol⁻¹). Additionally, each stable conformer was subjected to frequency calculations at the B3LYP/6-31G(d) level of theory to confirm their identities as being true minima.

2.3. Solvation Effects. The solvation effects were added using two continuum models: (i) isodensity polarizable continuum model (IPCM)²⁷ and (ii) Poisson–Boltzmann self-consistent reaction field (PB-SCRf) method.^{28,29}

(i) *Isodensity Polarizable Continuum Model (IPCM).* The effect of three different solvents (water, acetonitrile, and chloroform) was calculated by the IPCM method implemented in Gaussian 03. IPCM is more advanced than the polarizable continuum model (PCM) method⁴² because in IPCM the cavity of a solute is defined by the electron isodensity surface while the PCM method defines the cavity from a set of overlapping

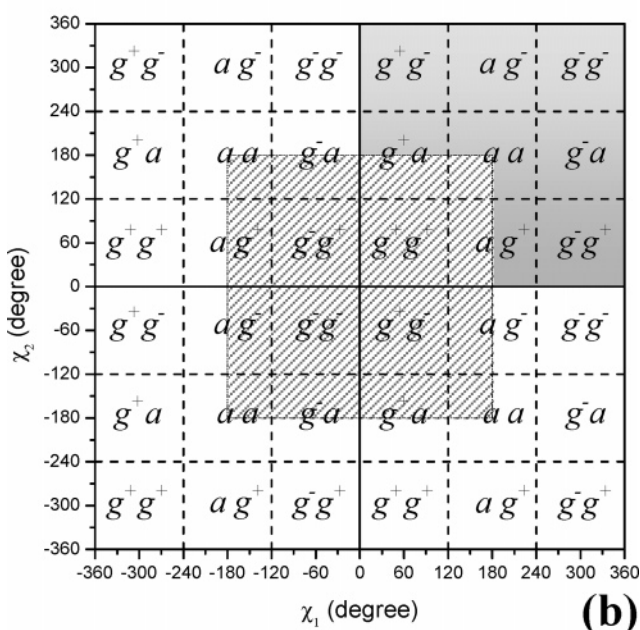
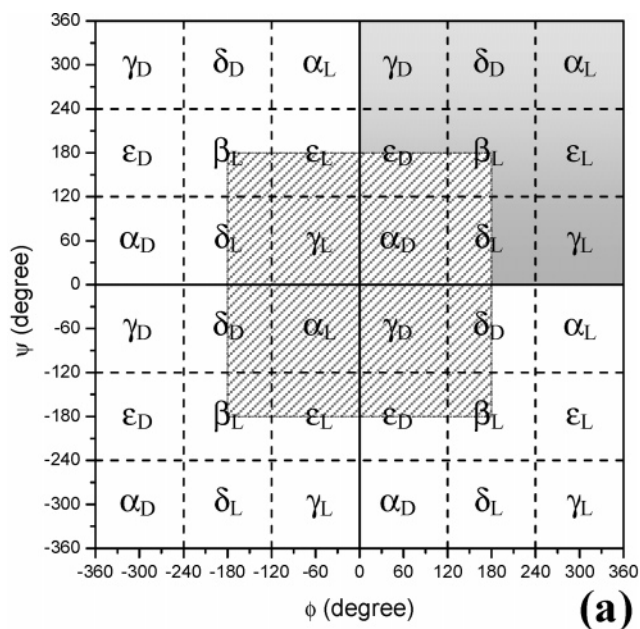


Figure 2. (a) Topological representation of the Ramachandran backbone potential energy surface (PES). (b) Topological representation of the side-chain PES. In both cases, the central box denoted by a hatched-lines area ($-180^\circ \leq \phi$ or $\chi_1 \leq 180^\circ$ and $-180^\circ \leq \psi$ or $\chi_2 \leq 180^\circ$) represents the cut suggested by the IUPAC convention. The quadrant denoted by a gray shaded area is the conventional or traditional cut ($0^\circ \leq \phi$ or $\chi_1 \leq 360^\circ$ and $0^\circ \leq \psi$ or $\chi_2 \leq 360^\circ$).

spherical atoms having the appropriate van der Waals radii. The efficiency of this method has been recognized in conformational behaviors in solution for small peptides.⁴³ It should be emphasized, however, that the evaluation of the solvent effect implies a comparison to the gas-phase results. The IPCM energies were obtained by single-point calculations over the gas-phase optimized geometries. Thus, both sets of results with and without the solvent are required.

(ii) *Poisson–Boltzmann Self-Consistent Reaction Field (PB-SCRf).* The effect of three different solvents (water, acetonitrile, and chloroform) was calculated by the Poisson–Boltzmann self-consistent reaction field (PB-SCRf) method incorporated in the Jaguar 5.5 program package.⁴⁴ The practical implementation of SCRf involves the synthesis of a polarizable quantum mechan-

ical solute and a continuum description of the solvent. First, the gas-phase electron density for the solute is determined and the resulting charge distribution is used to calculate atom-centered charges via an electrostatic potential (ESP) least squares fitting procedure. The gas-phase ESP charges are then passed to a Poisson–Boltzmann (PB) equation solver along with the van der Waals radii for each atom.²⁹ The radii are used to determine a solvent accessible surface, which defines the solute/solvent boundary. The interior solute region is assigned a dielectric constant of 1.00, and the exterior solvent region is assigned a dielectric of 78.39 for bulk water. The PB solver computes the charge distribution at the solute–solvent interface, which is then used to compute the solute–solvent part of the Hamiltonian. The interaction polarizes the solute and a new ESP charge distribution is then calculated and passed to the PB solver. The calculations are repeated until convergence is reached. In this model, the entire solute ESP charge was placed inside the solute cavity. Although some penetration of charges outside the cavity is unavoidable, this approximation has been shown to yield quite good results.^{29,45–48} PB-SCRF model geometries, energies, and frequencies were obtained by full optimization starting from the gas-phase geometry.

3. Results and Discussion

3.1. Gas Phase. The overall expression of the potential energy hypersurface (PEHS) for compound **I** is a function of eight variables $E = E(\omega_0, \phi, \psi, \omega_1, \chi_1, \chi_2, \chi_3, \chi_4)$. When limiting our considerations only to *trans*-peptide bonds (i.e., $\omega_0 \approx \omega_1 \approx 180^\circ$), the full conformational space will include six torsional angles, ϕ , ψ , χ_1 , χ_2 , χ_3 , and χ_4 , as defined in Figure 1. Thus, in principle, the conformational PEHS is a function of six variables:

$$E = E(\phi, \psi, \chi_1, \chi_2, \chi_3, \chi_4) \quad (1)$$

It should be noted that methyl rotations may be ignored due to the fact that the $-\text{CH}_3$ group has only one unique orientation. In fact, only two torsional angles in the SC need to be varied, and these are the torsional angles labeled χ_1 and χ_2 in **I**. Thus, the PEHS of **I** can be expressed as a function of only four independent variables.

$$E = E(\phi, \psi, \chi_1, \chi_2) \quad (2)$$

As three minima (g^+ , a , g^-) are expected for each variable according to MDCA,^{30–32} this would lead to the existence of $3^4 = 81$ conformers. These 81 conformers would be distributed evenly, namely, nine SC conformers for each of the nine BB structures. Using 81 MDCA-predicted geometries as input, a total of 62 conformers were located on the PEHS (eq 2) at the RHF/3-21G level of theory, instead of the 81 expected structures. The results of full optimization of the title compound at the RHF/3-21G level of theory including geometric parameters, total energies, and relative energies are given in Table S1 of the Supporting Information. Subsequent refinement of these stable conformers at the B3LYP/6-31G(d) level of theory resulted in 43 structures. The SC conformers found for each BB conformer are given in Figure 3a. The DFT results of geometry optimizations of the title compound at the B3LYP/6-31G(d) level of theory including geometric parameters, total energies, and relative energies are given in Table S2 of the Supporting Information. Figure S1, also available as Supporting Information, provides the spatial view of all optimized structures obtained at B3LYP/6-31G(d) level of theory.

DFT calculations predict the γ_L (ag^+) conformation as the global minimum. This BB conformation is folded (C_7^{eq} form),

and the side chain is partially folded. Considering an energy window of $2 \text{ kcal}\cdot\text{mol}^{-1}$, there are five γ_L forms (ag^+ , g^-a , aa , g^-g^+ , and ag^-) and one β_L conformation (g^-a). In other words, DFT calculations predict the γ_L (C_7^{eq}) and β_L (C_5) forms as the highly preferred conformations for the BB of compound **I** in the gas phase, showing a preference for the γ_L conformations. Table 1 shows the calculated relative populations in the gas phase for all BB types of compound **I**. Under thermodynamic equilibrium in the gas phase, the most populated BB conformer falls within the γ_L region (89.84%), whereas the β_L region has a relative population of 8.23%. Also, it should be noted that although extended (aa), partially folded (ag^+ , ag^- , and g^-a) and folded (g^-g^+) SC conformations were found for this energy gap of $2 \text{ kcal}\cdot\text{mol}^{-1}$, there is a conformational preference for the (ag^+) and (g^-a) SC orientations. Table 2 provides the calculated relative populations in gas phase for all SC types of compound **I**. The relative populations calculated for (ag^+) and (g^-a) SC orientations are 48.75% and 33.38%, respectively.

Examination of the relative energy differences obtained for the conformations of Leu allows a comparison between theoretical calculations reported here and previously reported experimental data obtained from X-ray^{49–53} studies. It is interesting to note that our theoretical calculations are in good agreement with the experimental data, fundamentally in relation to the SC orientation of the global minimum (ag^+) and the second local minimum (g^-a).

In most single amino acid systems using the diamide approximation, not all nine legitimate conformers will appear as energy minima on the Ramachandran PES.^{54–56} Most often the α_L and ϵ_L conformations are annihilated. Nevertheless, for Ile,¹⁹ Glu,²⁰ and Thr,⁵⁷ α_L and ϵ_L conformations were reported as energy minima on the Ramachandran PES at DFT level of theory. On the other hand, for Gln,²¹ Tyr,⁵⁸ and Trp⁵⁹ the α_L form appears as an energy minimum, but ϵ_L conformation was annihilated. Particularly noteworthy is the fact that, until now, Ile was the only reported nonpolar amino acid that contains stable conformers at all nine BB conformations using B3LYP/6-31G(d) calculations. Leu is the isomeric amino acid of Ile, having the only structural difference in the position of the SC branching. However, our results show that, for Leu, ϵ_L conformation is not an energy minimum on the Ramachandran PES whereas B3LYP/6-31G(d) calculations predict the existence of one conformer α_L (ag^-) that possesses $6.98 \text{ kcal}\cdot\text{mol}^{-1}$ above the global minimum.

Considering an energy window of $5 \text{ kcal}\cdot\text{mol}^{-1}$, there are 27 different conformations for Leu as well as for Ile, indicating a considerable conformational flexibility in both blocked single residues. Therefore, we might conclude that Ile and Leu show a similar conformational behavior, at least in the gas phase. However, solvent effect should be considered to reflect more reliable conformational preferences. Moreover, the geometry relaxation induced by the solvent on the solute molecules cannot often be neglected. Thus, in the next section we performed an energetic and conformational analysis taking into account the solvent effect in order to obtain more precise information about the conformational preferences adopted by compound **I**.

3.2. Solution. Theoretical studies on the effect of the solvent on the properties and behavior of molecules are at present performed according to a large variety of methods which can, however, refer to two basically different strategies: supermolecule and continuum approaches. The supermolecule approach includes explicit water molecules surrounding the solute. It provides information about the structure of the solvation layer, but a large number of water molecules is needed in order to

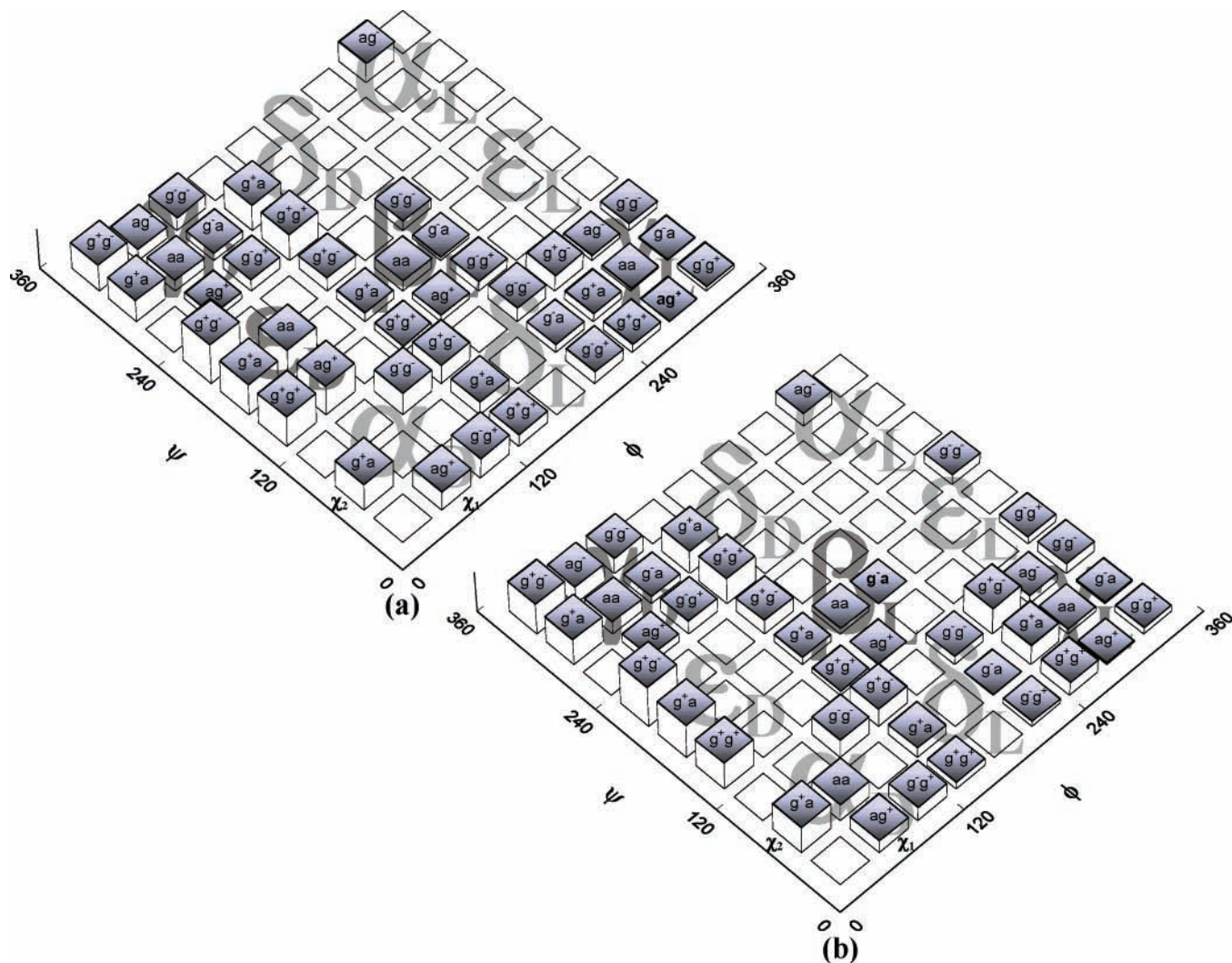


Figure 3. Schematic representation of the minima on the PEHS of four independent variables $E = E(\phi, \psi, \chi_1, \chi_2)$ for $\text{CH}_3\text{CO-Leu-NHCH}_3$. The global minimum is denoted by a bold symbol, and the energy gap above the global minimum is in relationship with the highest of the block. In this representation the traditional cut ($0^\circ \leq \phi \leq 360^\circ$ and $0^\circ \leq \psi \leq 360^\circ$) is used. (a) Minima obtained at B3LYP/6-31G(d) level of theory in vacuo. (b) Minima obtained at PB-SCRF/B3LYP/6-31G(d) level of theory in water ($\epsilon = 78.39$).

TABLE 1: Relative Population (%)^a in the Gas Phase and in Solution for Backbone (BB) Types of $\text{CH}_3\text{CO-Leu-NHCH}_3$, Computed at B3LYP/6-31G(d), IPCM/B3LYP/6-31G(d), and PB-SCRF/B3LYP/6-31G(d) Levels of Theory

BB types	B3LYP/6-31G(d) gas phase	IPCM/B3LYP/6-31G(d)			PB-SCRF/B3LYP/6-31G(d)			experimental
		chloroform ($\epsilon = 4.90$)	acetonitrile ($\epsilon = 36.64$)	water ($\epsilon = 78.39$)	chloroform ($\epsilon = 4.90$)	acetonitrile ($\epsilon = 36.64$)	water ($\epsilon = 78.39$)	
α_D	6.58×10^{-4}	0.04	0.28	0.31	0.01	0.05	0.14	0.93
ϵ_D	9.94×10^{-7}	9.77×10^{-6}	1.27×10^{-5}	1.14×10^{-5}	2.06×10^{-6}	2.00×10^{-5}	4.92×10^{-5}	0.23
γ_D	1.50	33.17	56.34	63.06	1.96	1.60	1.28	0.16
δ_D	7.77×10^{-6}	2.22×10^{-4}	1.03×10^{-3}	1.11×10^{-3}	4.50×10^{-5}	1.98×10^{-4}	3.77×10^{-4}	0.38
β_L	8.23	6.40	22.88	18.77	38.73	43.94	47.94	8.53
δ_L	0.43	6.01	11.24	11.40	3.96	15.88	20.08	2.50
γ_L	89.84	54.37	9.24	6.44	55.33	36.57	29.60	9.55
α_L	2.46×10^{-4}	6.06×10^{-3}	1.31×10^{-2}	1.24×10^{-2}	4.70×10^{-3}	0.06	0.05	52.75
ϵ_L	0.00	0.00	0.00	0.00	0.00	1.90	0.91	24.96

^a Populations are calculated from electronic energies (E_i) values of gas-phase, IPCM, and PB-SCRF calculations, i.e., $e^{-(E_i/RT)}/e^{-(E_{\text{min}}/RT)}$, where i corresponds to the i th conformer. Populations of conformers with the BB in the same catchment region are summed.

obtain a system more stable than the normal form since long-range interactions are neglected. Continuum models do not provide such information, but they include long-range interactions, which are important in the stabilization of the solute. Among the several approaches proposed to describe the solvent effect at the ab initio level, continuum models are quite popular due to their flexibility and efficiency.^{60–63} In such models the solute molecule, possibly supplemented by some solvent

molecules belonging to the first solvation shell, is placed in a cavity surrounded by a polarizable continuum, whose reaction field modifies the energy and the properties of the solute. In the most advanced ab initio models^{27,42,64–68} the cavities are of molecular shape, and the reaction field is described in terms of apparent polarization charges or reaction field factors included in the solute Hamiltonian, so it is possible to perform iterative procedures leading to self-consistency between the solute wave

TABLE 2: Relative Population (%)^a in the Gas Phase and in Solution for Side-Chain (SC) Types of CH₃CO-Leu-NHCH₃, Computed at B3LYP/6-31G(d), IPCM/B3LYP/6-31G(d), and PB-SCRF/B3LYP/6-31G(d) Levels of Theory

SC types	B3LYP/6-31G(d) gas phase	IPCM/B3LYP/6-31G(d)			PB-SCRF/B3LYP/6-31G(d)		
		chloroform ($\epsilon = 4.90$)	acetonitrile ($\epsilon = 36.64$)	water ($\epsilon = 78.39$)	chloroform ($\epsilon = 4.90$)	acetonitrile ($\epsilon = 36.64$)	water ($\epsilon = 78.39$)
g^+, g^+	1.04	0.80	0.32	0.25	3.61	4.63	3.47
g^+, a	0.57	0.84	0.20	0.14	1.15	1.17	0.90
g^+, g^-	0.03	6.45×10^{-3}	5.53×10^{-4}	3.66×10^{-4}	0.07	0.09	0.07
a, g^+	48.75	54.35	81.20	83.10	39.79	33.48	34.16
a, a	9.14	3.09	0.70	0.53	4.44	4.30	3.95
a, g^-	3.00	2.32	0.40	0.29	0.75	0.44	0.58
g^-, g^+	3.17	2.66	1.63	1.42	3.21	4.90	4.06
g^-, a	33.38	34.39	14.79	13.60	46.25	50.47	51.95
g^-, g^-	0.92	1.53	0.76	0.67	0.72	0.53	0.86

^a Populations are calculated from electronic energies (E_i) values of gas-phase, IPCM, and PB-SCRF calculations, i.e., $e^{-(E_i/RT)}/e^{-(E_{\min}/RT)}$, where i corresponds to the i th conformer. Populations of conformers with the SC in the same catchment region are summed.

TABLE 3: Relative Energies^a for the Conformations of CH₃CO-Leu-NHCH₃ with $\Delta E_{\text{rel}} \leq 5.00$ kcal·mol⁻¹^b

B3LYP/6-31G(d)		IPCM/B3LYP/6-31G(d)						PB-SCRF/B3LYP/6-31G(d)					
gas phase		chloroform ($\epsilon = 4.90$)		acetonitrile ($\epsilon = 36.64$)		water ($\epsilon = 78.39$)		chloroform ($\epsilon = 4.90$)		acetonitrile ($\epsilon = 36.64$)		water ($\epsilon = 78.39$)	
conf	ΔE_{rel}	conf	ΔE_{rel}	conf	ΔE_{rel}	conf	ΔE_{rel}	conf	ΔE_{rel}	conf	ΔE_{rel}	conf	ΔE_{rel}
$\gamma_L(a, g^+)$	0.00	$\gamma_D(a, g^+)$	0.00	$\gamma_D(a, g^+)$	0.00	$\gamma_D(a, g^+)$	0.00	$\gamma_L(a, g^+)$	0.00	$\beta_L(g^-, a)$	0.00	$\beta_L(g^-, a)$	0.00
$\gamma_L(g^-, a)$	0.33	$\gamma_L(g^-, a)$	0.15	$\beta_L(a, g^+)$	0.53	$\beta_L(a, g^+)$	0.71	$\beta_L(g^-, a)$	0.15	$\gamma_L(a, g^+)$	0.13	$\beta_L(a, g^+)$	0.08
$\gamma_L(a, a)$	0.95	$\gamma_L(a, g^+)$	0.23	$\delta_L(g^-, a)$	1.00	$\delta_L(g^-, a)$	1.05	$\gamma_L(g^-, a)$	0.25	$\beta_L(a, g^+)$	0.29	$\delta_L(g^-, a)$	0.19
$\beta_L(g^-, a)$	1.18	$\delta_L(g^-, a)$	1.06	$\gamma_L(g^-, a)$	1.51	$\gamma_L(g^-, a)$	1.78	$\beta_L(a, g^+)$	0.66	$\delta_L(g^-, a)$	0.33	$\gamma_L(a, g^+)$	0.30
$\gamma_L(g^-, g^+)$	1.58	$\beta_L(g^-, a)$	1.15	$\gamma_L(a, g^+)$	1.59	$\gamma_L(a, g^+)$	1.88	$\gamma_L(a, a)$	1.21	$\gamma_L(g^-, a)$	0.34	$\gamma_L(g^-, a)$	0.39
$\gamma_L(a, g^-)$	1.70	$\gamma_L(a, a)$	1.45	$\delta_L(g^-, g^+)$	2.12	$\delta_L(g^-, g^+)$	2.25	$\beta_L(g^+, g^+)$	1.24	$\beta_L(g^+, g^+)$	1.02	$\beta_L(g^+, g^+)$	1.26
$\beta_L(a, g^+)$	2.23	$\gamma_L(a, g^-)$	1.51	$\beta_L(g^-, a)$	2.44	$\beta_L(g^-, a)$	2.70	$\delta_L(g^-, a)$	1.28	$\gamma_L(a, a)$	1.20	$\gamma_L(a, a)$	1.31
$\gamma_D(a, g^+)$	2.24	$\beta_L(a, g^+)$	1.72	$\gamma_L(a, a)$	2.85	$\gamma_L(a, a)$	3.10	$\gamma_L(g^-, g^+)$	1.57	$\epsilon_L(g^-, g^+)$	1.47	$\delta_L(g^-, g^+)$	1.37
$\gamma_L(g^-, g^-)$	2.36	$\gamma_L(g^-, g^+)$	1.78	$\gamma_L(a, g^-)$	2.85	$\gamma_L(a, g^-)$	3.13	$\beta_L(g^+, a)$	1.88	$\delta_L(g^-, g^+)$	1.55	$\beta_L(a, a)$	1.56
$\beta_L(g^+, g^+)$	2.39	$\gamma_L(g^-, g^-)$	1.87	$\gamma_L(g^-, g^-)$	2.92	$\gamma_L(g^-, g^-)$	3.16	$\gamma_D(g^-, a)$	1.96	$\gamma_L(g^-, g^+)$	1.62	$\gamma_L(g^-, g^+)$	1.72
$\gamma_D(g^-, a)$	2.65	$\delta_L(g^-, g^+)$	2.04	$\gamma_L(g^+, g^+)$	2.98	$\gamma_L(g^+, g^+)$	3.18	$\gamma_D(a, g^+)$	2.07	$\beta_L(a, a)$	1.67	$\delta_L(g^+, g^+)$	1.88
$\delta_L(g^-, a)$	2.81	$\gamma_D(g^-, a)$	2.13	$\gamma_D(a, a)$	3.04	$\gamma_D(a, a)$	3.21	$\beta_L(a, a)$	2.09	$\beta_L(g^+, a)$	1.79	$\beta_L(g^+, a)$	1.99
$\gamma_L(g^+, a)$	2.85	$\gamma_L(g^+, g^+)$	2.17	$\gamma_D(g^-, a)$	3.40	$\alpha_D(g^-, g^-)$	3.53	$\gamma_L(a, g^-)$	2.13	$\gamma_D(g^-, a)$	1.97	$\epsilon_L(g^-, g^+)$	2.00
$\gamma_L(g^+, g^+)$	2.93	$\gamma_L(g^+, a)$	2.22	$\gamma_L(g^+, a)$	3.44	$\gamma_D(g^-, a)$	3.66	$\beta_L(g^-, g^+)$	2.18	$\delta_L(g^+, g^+)$	2.06	$\gamma_D(g^-, a)$	2.01
$\beta_L(g^-, a)$	3.07	$\gamma_D(a, a)$	2.49	$\gamma_D(g^-, g^+)$	3.44	$\gamma_D(g^-, g^+)$	3.68	$\delta_L(g^-, g^+)$	2.29	$\gamma_D(g^-, a)$	2.08	$\gamma_L(a, g^-)$	2.18
$\beta_L(g^-, g^+)$	3.39	$\gamma_D(g^-, g^+)$	2.94	$\gamma_D(g^-, g^-)$	3.49	$\gamma_L(g^+, a)$	3.70	$\beta_L(g^-, g^-)$	2.59	$\gamma_L(a, g^-)$	2.42	$\gamma_D(a, g^+)$	2.24
$\beta_L(g^-, g^-)$	3.39	$\gamma_D(g^-, g^-)$	3.00	$\alpha_D(g^-, g^-)$	3.52	$\gamma_L(g^-, g^+)$	3.75	$\gamma_L(g^-, g^-)$	2.59	$\delta_L(g^-, g^-)$	2.64	$\delta_L(g^-, g^-)$	2.24
$\beta_L(a, a)$	3.73	$\beta_L(a, a)$	3.08	$\gamma_D(g^-, g^+)$	3.76	$\gamma_D(g^-, g^+)$	3.97	$\delta_L(g^+, g^+)$	3.01	$\gamma_L(g^-, g^-)$	2.75	$\epsilon_L(g^-, g^-)$	2.72
$\gamma_D(a, a)$	3.79	$\delta_L(g^+, a)$	3.12	$\delta_L(g^+, a)$	3.99	$\delta_L(g^+, a)$	4.19	$\gamma_D(a, a)$	3.45	$\delta_L(g^+, a)$	3.03	$\delta_L(g^+, g^-)$	2.78
$\gamma_D(g^-, g^+)$	4.01	$\delta_L(g^+, a)$	3.29	$\beta_L(a, a)$	4.38	$\beta_L(a, a)$	4.65	$\gamma_D(g^-, g^+)$	3.46	$\gamma_D(a, a)$	3.18	$\delta_L(g^+, a)$	2.81
$\gamma_D(a, g^-)$	4.23	$\beta_L(g^-, g^-)$	3.31	$\beta_L(g^-, g^-)$	4.66	$\alpha_D(a, g^+)$	4.88	$\delta_L(g^-, g^-)$	3.56	$\epsilon_L(g^-, g^-)$	3.29	$\gamma_D(a, a)$	3.41
$\delta_L(g^+, g^+)$	4.25	$\beta_L(g^+, a)$	3.50	$\beta_L(g^-, g^+)$	4.68	$\alpha_L(a, g^-)$	4.90	$\beta_L(g^+, g^-)$	3.85	$\gamma_D(g^-, g^+)$	3.30	$\alpha_D(a, g^+)$	3.44
$\delta_L(g^+, g^+)$	4.28	$\beta_L(g^+, g^+)$	3.69	$\alpha_D(a, g^+)$	4.79	$\beta_L(g^-, g^-)$	4.92	$\gamma_L(g^+, g^+)$	3.99	$\alpha_L(a, g^+)$	3.42	$\alpha_L(a, g^-)$	3.50
$\delta_L(g^+, a)$	4.69	$\gamma_D(a, g^-)$	4.19	$\alpha_L(a, g^-)$	4.80	$\beta_L(g^-, g^+)$	4.98	$\delta_L(g^+, a)$	4.02	$\beta_L(g^+, g^-)$	3.53	$\gamma_D(g^-, g^+)$	3.56
$\beta_L(g^+, g^-)$	4.75	$\delta_L(g^+, g^+)$	4.24					$\gamma_D(a, g^-)$	4.13	$\gamma_D(a, g^-)$	3.76	$\alpha_D(a, g^+)_2$	3.67
$\gamma_D(g^-, g^-)$	4.78	$\delta_L(g^-, g^-)$	4.30					$\gamma_D(g^-, g^-)$	4.35	$\alpha_D(g^-, g^+)$	3.97	$\gamma_L(g^+, g^+)$	3.76
$\delta_L(g^-, g^-)$	4.94	$\alpha_D(g^-, g^-)$	4.45					$\gamma_L(g^+, a)$	4.60	$\alpha_D(a, g^+)$	4.12	$\beta_L(g^+, g^-)$	3.83
		$\alpha_L(a, g^-)$	4.92							$\gamma_D(g^-, g^-)$	4.18	$\alpha_D(g^-, g^+)$	3.84
		$\alpha_D(a, g^+)$	4.94							$\gamma_L(g^+, g^+)$	4.45	$\gamma_D(g^-, g^-)$	4.41
												$\alpha_D(a, a)$	4.59
												$\gamma_D(a, g^-)$	4.72
												$\delta_L(g^+, g^-)$	4.89
												$\alpha_D(g^-, g^-)$	4.96

^a Relative energies in kcal·mol⁻¹; total energy values are available as Supporting Information (Tables S1–S6). ^b Obtained at B3LYP/6-31G(d), IPCM/B3LYP/6-31G(d), and PB-SCRF/B3LYP/6-31G(d) levels of theory. Three different solvents are simulated.

function and the solvent polarization. Moreover, the geometry relaxation induced by the solvent on the solute molecules cannot often be neglected; thus, an efficient solvation model must provide energy gradients and allow geometry optimizations in solution. In other words, it is desirable that both direct (i.e., polarization) and indirect (i.e., relaxation) solvent effects be treated with the same accuracy. Therefore, in the present analysis, besides the IPCM model²⁷ we also adopt the Poisson–Boltzmann self-consistent reaction field (PB-SCRF) methodology^{28,29} in order to obtain relaxed geometries of leucine in solution. The entire behavior of Leu in solution is not expected to be explained by such a reduced treatment. Our aim in this study is less ambitious: we wish to obtain a reasonable indication of the direction and magnitude of changes in the

conformational preferences of the isolated molecule when it enters different solutions, and from this point of view, the inclusion of three solvents in the computations with different dielectric constants should be particularly significant.

When the solvent effect was applied with the IPCM method, the relative energies of stable conformers for Leu in solution were significantly different from those in the gas phase (Table 3 and Figure 4). The γ_D , β_L , and δ_L conformations were stabilized in solution irrespective of the solvent type. Thus, the most notable change observed corresponds to the $\gamma_D(ag^+)$ form. This conformation possesses 2.24 kcal·mol⁻¹ above the global minimum in vacuo, but it becomes the global minimum in solution for the three solvents used. Table 1 reports the calculated relative populations in solution using the IPCM

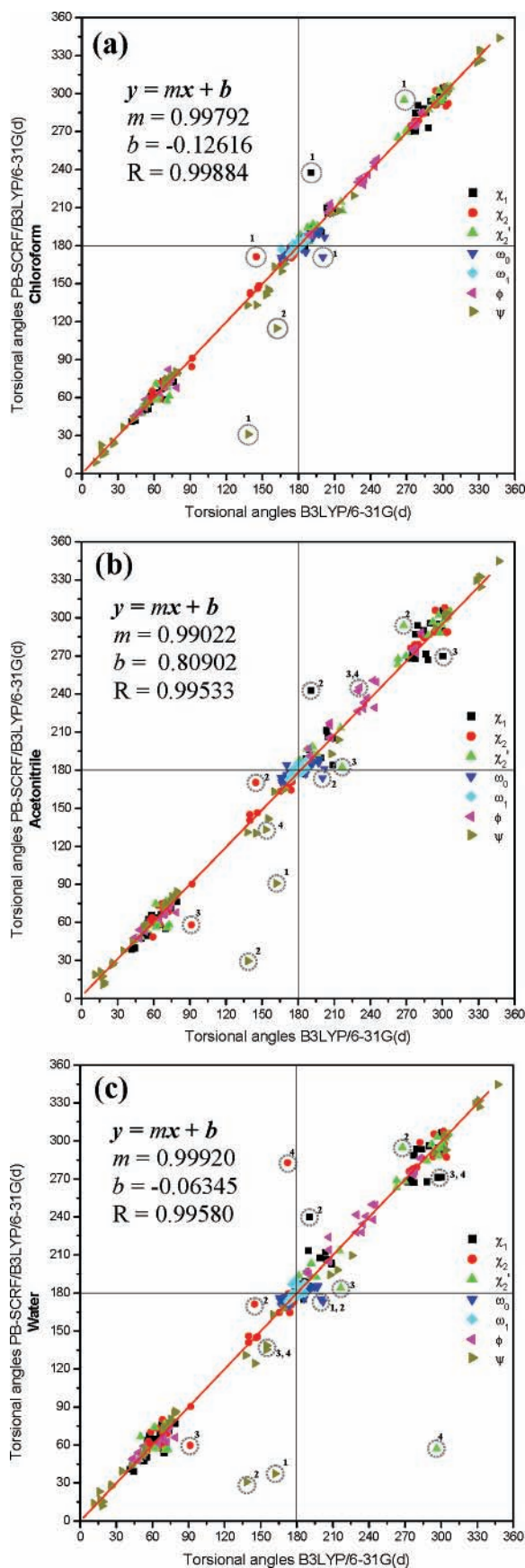


Figure 5. Correlation of torsional angles computed at B3LYP/6-31G(d) and PB-SCRF/B3LYP/6-31G(d) levels of theory for $\text{CH}_3\text{CO-Leu-NHCH}_3$. Three different solvents were simulated: (a) chloroform ($\epsilon = 4.90$), (b) acetonitrile ($\epsilon = 36.64$), and (c) water ($\epsilon = 78.39$). Those points labeled 1–4 were omitted from the least-squares fit.

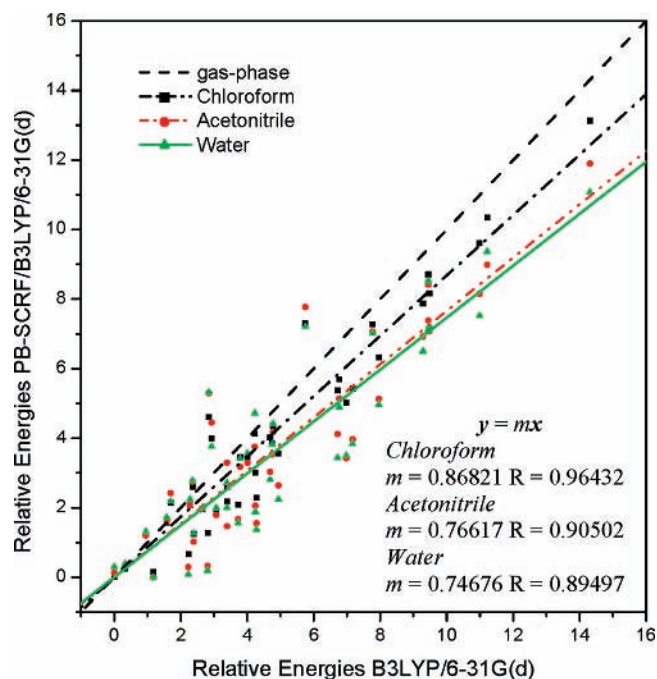


Figure 6. Correlation of relative energies computed at B3LYP/6-31G(d) and PB-SCRF/B3LYP/6-31G(d) levels of theory for $\text{CH}_3\text{CO-Leu-NHCH}_3$. Three different solvents were simulated: chloroform ($\epsilon = 4.90$), acetonitrile ($\epsilon = 36.64$), and water ($\epsilon = 78.39$).

the intrinsic interactions of α -helix structure which play a crucial role in its stabilization.

Tables S4–S6, which are available as Supporting Information, provide geometric parameters, total energies, and relative energies calculated for the title compound at PB-SCRF/B3LYP/6-31G(d) level of theory in chloroform ($\epsilon = 4.90$), acetonitrile ($\epsilon = 36.64$), and water ($\epsilon = 78.39$), respectively. Taking into account that the PB-SCRF method includes geometric relaxation, a few conformational changes were found when the solvent effect was taken into account for any of the solvents here used. Thus, $\epsilon_D(ag^+)$ and $\epsilon_D(aa)$ forms seem to be unstable in chloroform and water solution since their BB conformations turn to the α_D form keeping the same side-chain orientation (Figure 5a,c, points labeled 1 and 2). Moreover, $\beta_L(g^-g^+)$ and $\beta_L(g^-g^-)$ conformers experience a slight change in the value of ϕ torsional angle, sufficient to shift to $\epsilon_L(g^-g^+)$ and $\epsilon_L(g^-g^-)$, respectively (Figure 5b,c, points labeled 3 and 4). The former behavior was observed only in acetonitrile and water environments. The full correlation of the torsional angles (in the present case, ϕ , ψ , χ_1 , χ_2 , ω_0 , and ω_1) computed in solution using the three different solvents for the title compound is shown in Figure 5. The least-squares fit was of the $y = mx + b$ type. Neither m is unity nor b is zero for any of the solvents here selected. Thus, the fitted lines show a good correlation suggesting that some geometric changes were observed when the PB-SCRF method was applied. It is also notable that the geometric changes are only slightly in the solvents ($\epsilon = 4.90$ – 78.39) but are rather different from those in vacuo. It is prudent, at this time, to make a comparison of the relative energies obtained in solution and the gas phase. The relative energies (ΔE_{rel}) of the title compound, computed in three different solvents, are compared in Figure 6. Since the global minimum, on the relative energy scale, is always zero by definition, a $y = mx$ equation was fitted to the data points so that the fitted line passes over the origin. Although the slopes of the fitted lines are never unity, it is clear that the PB-SCRF/B3LYP/6-31G(d) results in chloroform reproduce the trend quite well. However,

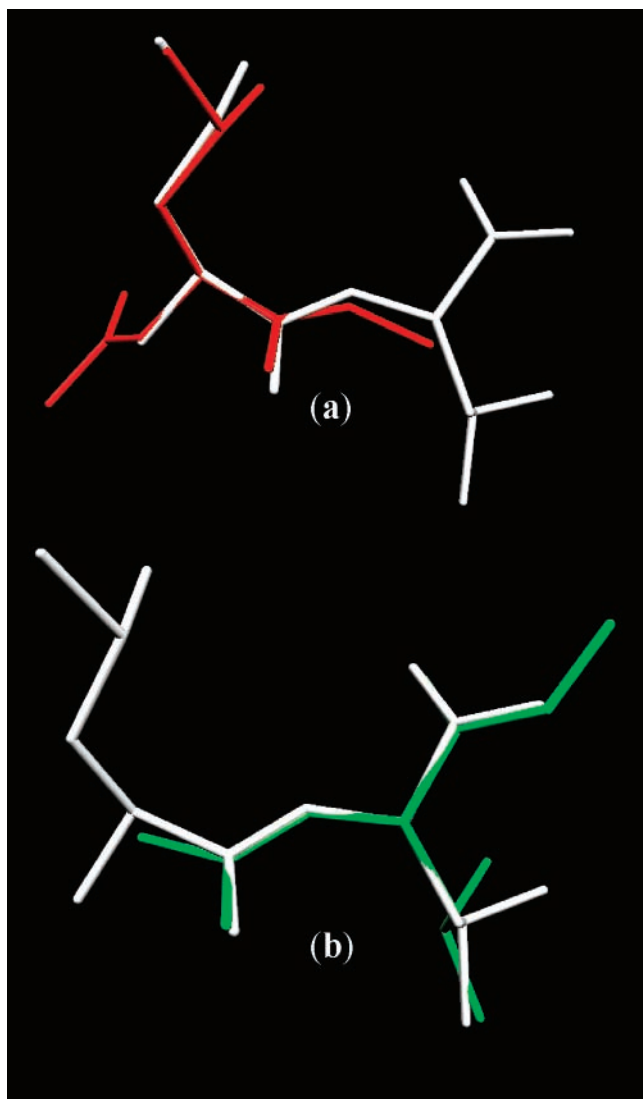


Figure 7. Overlapped stereoviews of the structure reported in ref 69 in white and two conformations obtained for $\text{CH}_3\text{CO-Leu-NHCH}_3$ at PB-SCRF/B3LYP/6-31G(d) level of theory in water. (a) β_L (ag^+) in red; (b) β_L (g^+g^+) in green. All hydrogens are omitted for clarity.

the tendency of the relative energies exhibited in acetonitrile and water suggest a fairly different conformational preference from that observed in the gas phase. Figure S2, which is available as Supporting Information, provides the spatial view of optimized structures obtained at PB-SCRF/B3LYP/6-31G(d) level of theory in water.

The validity of PB-SCRF calculations might be assessed by comparing the predicted structures with those derived experimentally, by either X-ray crystallographic⁶⁹ or IR⁷⁰ studies. It is interesting to mention that our theoretical calculations are in agreement with these experimental data. Particularly, it is worthwhile to compare the preferred conformations obtained at PB-SCRF/B3LYP/6-31G(d) level of theory in water with those previously reported from X-ray studies.⁶⁹ Mitra et al. reported the crystal structure of a dipeptide L-leucyl-L-leucine which adopts an extended (β_L) backbone conformation, whereas, for the first leucyl residue, the side-chain orientation corresponds to an (ag^+) form and the second leucyl residue adopts a sterically unfavorable (g^+g^+) conformation. These results are closely related to those reported here as the predominant aqueous conformations. Thus, β_L (ag^+) form is our second local minimum ($\Delta E = 0.08 \text{ kcal}\cdot\text{mol}^{-1}$) and β_L (g^+g^+) conformation

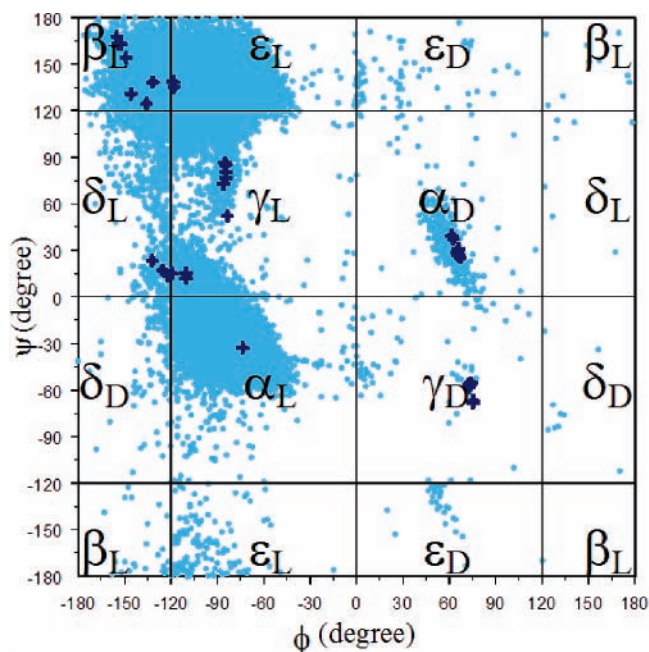


Figure 8. Backbone conformers of all 39 494 Leu residues taken from 1395 nonhomologous proteins. Using their backbone dihedral parameters, all of the above Leu residues were plotted on a $[\phi, \psi]$ map (in light blue). Locations of Leu backbone conformers obtained at PB-SCRF/B3LYP/6-31G(d) level of theory in water ($\epsilon = 78.39$) in an energy window of $5 \text{ kcal}\cdot\text{mol}^{-1}$ are also shown (in dark blue).

displays an energy gap of $1.26 \text{ kcal}\cdot\text{mol}^{-1}$ (sixth minimum) above the global minimum in water. In Figure 7 we overlapped the structure reported by Mitra et al. (in white) with two conformations obtained for Leu at PB-SCRF/B3LYP/6-31G(d) level of theory in water. In this figure it can be appreciated that the first leucyl residue (Figure 7a) shows a complete overlap, not only with the backbone but also with the side chain. Also, for the second leucyl residue (Figure 7b), although there is not a complete fit, the resemblance is still apparent.

3.3. Correlation between Experimental Data and Computed Stability. Although the results reported here using diverse approaches are comparable, they displayed some differences, in particular with respect to the preferred conformations suggested by the different methods. At this stage of our work we consider it a reasonable step to take a look for an arbitrage by experimental results. Thus, to better understand the above theoretical results, we performed a comparison of structural parameters (torsional angles) from experimental databases (X-ray and NMR) with our DFT results. To keep the modeling as simple as possible, it will be assumed that the probability of each conformer in proteins depends only on its relative energy. Obviously, in this model several well-known phenomena are neglected, such as inter-residue interactions and long-range effects. However, we believe that it is possible to correlate, in a simple way, the relative energies and the relative probabilities in an ensemble of proteins. Thus the former correlation by using a nonhomologous database is a potential technique for the cross-validation of the two approaches.

Using a recent (November 2006) X-ray and NMR determined protein data set of nonhomologous proteins,⁷¹ a population distribution map was generated. The backbone conformers of all 39 494 Leu residues, found in a total of 1395 nonhomologous proteins (99.29% trans and 0.71% cis conformers), were plotted showing ϕ against ψ values (Figure 8). To perform a comparison between calculated and observed backbone conformers, an additional plot was made with the SCRF/B3LYP/6-31G(d)

results obtained in water ($\epsilon = 78.39$). Comparison of these data sets shows an overall emerging promising similarity. The experimental (X-ray and NMR) data indicate highly populated zones: the first one corresponds to the α_L (right-handed α -helix) with 52.75% of the total population and the second one corresponds to the ϵ_L region with 24.96% of the total population. As can be seen in Table 1, neither α_L nor ϵ_L BB forms exhibit high calculated populations. As previously stated, this conformational discrepancy could be attributed to the limitations of the dipeptide approximation to describe the intrinsic interactions which play a crucial role in the stabilization of these BB types. The following most populated regions correspond to the γ_L (inverse γ -turn), β_L (extended β -strand), and δ_L BB conformations with 9.55%, 8.53%, and 2.50%, respectively. It is interesting to note that SCRf/B3LYP/6-31G(d) calculations obtained in water ($\epsilon = 78.39$) predict the β_L (47.94%), γ_L (29.60%), and δ_L (20.08%) BB conformations as the energetically preferred conformers (Table 1). From the results shown in Figure 8 it is clear that theoretical calculations are in complete agreement with experimental data. Such a correlation permits us to assume that although the diamide model does not reproduce some BB conformations with high accuracy, it is a good approximation to describe and predict, at least in part, the main protein chain folding.

4. Conclusions

We investigated the conformational preference of *N*-acetyl-L-leucine-*N'*-methylamide (**I**) using the ab initio and DFT methods and the advanced solute-treatment IPCM and PB-SCRf models. The relatively stable conformers of compound **I** were examined in gas and solution phases, and the relative energies of stable conformers depended significantly on solvation methods as well as medium phase.

The exploration of the full conformational space of compound **I**, considering nine backbone (along ϕ and ψ) and nine side-chain (along χ_1 and χ_2) geometries leading to $9 \times 9 = 81$ conformations, has been investigated. Geometry optimizations initially carried out at the RHF/3-21G level of theory were subsequently refined at the B3LYP/6-31G(d) level of theory, resulting in 43 stable conformers in the gas phase. DFT calculations predict the γ_L (C_7^{eq}) and β_L (C_5) forms as the highly preferred conformations for the backbone of compound **I**, showing a preference for the γ_L conformations. Also, there is a conformational preference for the (ag^+) and (g^-a) side-chain orientations. All these theoretical results are in good agreement with the experimental X-ray data.

Comparing the results obtained for compound **I** with Ile, a nonpolar amino acid previously reported, a similar conformational flexibility was found in both blocked single residues. However, for Ile all nine backbone conformations exhibited energy minimum forms whereas only eight backbone conformers were obtained for Leu as the ϵ_L backbone conformation was annihilated at all side-chain orientations in the gas phase.

The solvent effects observed in the IPCM results of compound **I** suggest the following: (1) that the conformational preferences change only slightly in acetonitrile ($\epsilon = 36.64$) and water ($\epsilon = 78.39$) but are significantly different from those in vacuo and chloroform ($\epsilon = 4.90$); (2) that the γ_D , β_L , and δ_L conformations are stabilized in solution irrespective of the solvent type; (3) that the γ_D (ag^+) form is the global minimum for the three solvents used; (4) that a high conformational flexibility was observed for Leu in solution, as well as in vacuo. The former result is in agreement with that previously reported for Ile.

The PB-SCRf results show that solvation plays an important role in the stability of β_L backbone forms in the three solvents

here used. Thus, β_L (g^-a) form is the global minimum in acetonitrile and water. However, the effects of solvent polarity are rather small in chloroform ($\epsilon = 4.90$) since γ_L (ag^+) conformation is the global minimum in this solvent, as well as in vacuo. Moreover, γ_L (C_7^{eq}) and δ_L (β_2) backbone forms are also favored. In a very good agreement with the experimental results reported by Mitra et al., the PB-SCRf model predicts an extended backbone conformation with (ag^+) side-chain orientation in aqueous solution. On the other hand, the α_L and ϵ_L backbone forms are only moderately stabilized in solution for the PB-SCRf method. Some plausible explanation could be the lack of ability of the dipeptide approximation to describe the intrinsic interactions of these backbone motifs. However, the correlation by using a nonhomologous protein database and the results obtained using the PB-SCRf method are in good agreement in spite of the limitations of the above-mentioned approximation.

It is interesting to note that although there were no substantial conformational changes, remarkably different conformational preferences were exhibited using the PB-SCRf method. It is also notable that the geometric changes are only slight in the solvents ($\epsilon = 4.90$ – 78.39) but are rather different from those in vacuo. Thus, this peptide model study shows that the inclusion of the geometric relaxation seems to be essential to carry out an extensive study of the solvent effects. Therefore, the possibility to reoptimize the molecular geometry of Leu taking the solvent effect into account sensibly improves the quality of the energy description and electronic properties of this system in solution.

Acknowledgment. This work was supported by grants from Universidad Nacional de San Luis (UNSL) and Consejo Nacional de Investigaciones Científicas y Técnicas (CONICET) of Argentina. R.D.E. is a member of the scientific staff of CONICET (Argentina). M.F.M. is a fellow of CONICET (Argentina). S.L. and R.F.M. thank support from the NIH-INBRE program, grant number: P20 RR016469.

Supporting Information Available: Table S1, torsional angles and total energy values for backbone and side-chain conformers optimized at RHF/3-21G level of theory; Table S2, torsional angles and total energy values for backbone and side-chain conformers optimized at B3LYP/6-31G(d) level of theory; Table S3, total energy values and calculated relative energies for all the conformations obtained at IPCM/B3LYP/6-31G(d) level of theory in three different solvents; Table S4, torsional angles and total energy values for backbone and side-chain conformers optimized at PB-SCRf/B3LYP/6-31G(d) level of theory using chloroform ($\epsilon = 4.90$) as solvent; Table S5, torsional angles and total energy values for backbone and side-chain conformers optimized at PB-SCRf/B3LYP/6-31G(d) level of theory using acetonitrile ($\epsilon = 36.64$) as solvent; and Table S6, torsional angles and total energy values for backbone and side-chain conformers optimized at PB-SCRf/B3LYP/6-31G(d) level of theory using water ($\epsilon = 78.39$) as solvent. Figure S1, conformers of $\text{CH}_3\text{CO-Leu-NHCH}_3$ optimized at B3LYP/6-31G(d) level of theory; Figure S2, conformers of $\text{CH}_3\text{CO-Leu-NHCH}_3$ optimized at PB-SCRf/B3LYP/6-31G(d) level of theory using water ($\epsilon = 78.39$). This material is available free of charge via the Internet at <http://pubs.acs.org>.

References and Notes

- (1) Zimmerman, S. S.; Pottle, M. S.; Némethy, G.; Scheraga, H. A. *Macromolecules* **1977**, *10*, 1.
- (2) O'Neil, K. T.; DeGrado, W. F. *Science* **1990**, *250*, 646.

- (3) Rooman, M. J.; Kocher, J.-P. A.; Wodak, S. J. *Biochemistry* **1992**, *31*, 10226.
- (4) Blaber, M.; Zhang, X.; Matthews, B. W. *Science* **1993**, *260*, 1637.
- (5) Brooks, C. L., III; Case, D. A. *Chem. Rev.* **1993**, *93*, 2487.
- (6) Street, A. G.; Mayo, S. L. *Proc. Natl. Acad. Sci. U.S.A.* **1999**, *96*, 9074.
- (7) Koehl, P.; Levitt, M. *Proc. Natl. Acad. Sci. U.S.A.* **1999**, *96*, 12524.
- (8) Ostroy, S. E.; Lotan, N.; Ingwall, R. T.; Scheraga, H. A. *Biopolymers* **1970**, *9*, 749.
- (9) Snell, C. R.; Fasman, G. D. *Biopolymers* **1972**, *11*, 1723.
- (10) Chou, P. Y.; Fasman, G. D. *J. Mol. Biol.* **1973**, *74*, 263.
- (11) Bychkova, V. E.; Gudkov, A. T.; Miller, W. G.; Mitin, Y. V.; Pitsyn, O. B.; Shpungin, I. L. *Biopolymers* **1975**, *14*, 1739.
- (12) Chou, P. Y.; Fasman, G. D. *Biochemistry* **1974**, *13*, 211.
- (13) Chou, P. Y.; Fasman, G. D. *Biochemistry* **1974**, *13*, 222.
- (14) Kubota, S.; Fasman, G. D. *Biopolymers* **1975**, *14*, 605.
- (15) Pederson, D.; Gabriel, D.; Hermans, J., Jr. *Biopolymers* **1971**, *10*, 2133.
- (16) Lotan, N.; Berger, A.; Katchalski, E. *Annu. Rev. Biochem.* **1972**, *41*, 869.
- (17) Ananthanarayanan, V. S. *J. Sci. Ind. Res.* **1972**, *31*, 593.
- (18) Arfmann, H.-A.; Labitzke, R.; Wagner, K. G. *Biopolymers* **1975**, *14*, 1381.
- (19) Rodríguez, A. M.; Koo, J. C. P.; Rojas, D. E.; Peruchena, N. M.; Enriz, R. D. *Int. J. Quantum Chem.* **2006**, *106*, 1580.
- (20) Masman, M. F.; Zamora, M. A.; Rodríguez, A. M.; Fidanza, N. G.; Peruchena, N. M.; Enriz, R. D.; Csizmadia, I. G. *Eur. Phys. J. D* **2002**, *20*, 531.
- (21) Klipfel, M. W.; Zamora, M. A.; Rodríguez, A. M.; Fidanza, N. G.; Enriz, R. D.; Csizmadia, I. G. *J. Phys. Chem. A* **2003**, *107*, 5079.
- (22) Alemán, C. *J. Phys. Chem. A* **2000**, *104*, 7612.
- (23) Padmanabhan, S.; Baldwin, R. L. *J. Mol. Biol.* **1994**, *241*, 706.
- (24) Creamer, T. P.; Rose, G. D. *Protein Sci.* **1995**, *4*, 1305.
- (25) Kobayashi, K.; Yonezawa, N.; Katakai, R. *Macromolecules* **1995**, *28*, 8242.
- (26) Padmanabhan, S.; Jiménez, M. A.; Laurents, D. V.; Rico, M. *Biochemistry* **1998**, *37*, 17318.
- (27) Foresman, J. B.; Keith, T. A.; Wiberg, K. B.; Snoonian, J. *J. Phys. Chem.* **1996**, *100*, 16098.
- (28) Tannor, D. J.; Marten, B.; Murphy, R.; Friesner, R. A.; Sitkoff, D.; Nicholls, A.; Ringnalda, M.; Goddard, W. A., III; Honig, B. *J. Am. Chem. Soc.* **1994**, *116*, 11875.
- (29) Marten, B.; Kim, K.; Cortis, C.; Friesner, R. A.; Murphy, R. B.; Ringnalda, M. N.; Sitkoff, D.; Honig, B. *J. Phys. Chem.* **1996**, *100*, 11775.
- (30) Peterson, M. R.; Csizmadia, I. G. *J. Am. Chem. Soc.* **1978**, *100*, 6911.
- (31) Peterson, M. R.; Csizmadia, I. G. *Prog. Theor. Org. Chem.* **1982**, *3*, 190.
- (32) Csizmadia, I. G. *New Theoretical Concept for Understanding Organic Reactions*; Csizmadia, I. G., Bertran, J. D., Eds.; Reidel: Dordrecht, The Netherlands, 1989.
- (33) IUPAC-IUB Commission on Biochemical Nomenclature. *Biochemistry* **1970**, *9*, 3471.
- (34) Frisch, M. J.; Trucks, G. W.; Schlegel, H. B.; Scuseria, G. E.; Robb, M. A.; Cheeseman, J. R.; Montgomery, J. A., Jr.; Vreven, T.; Kudin, K. N.; Burant, J. C.; Millam, J. M.; Iyengar, S. S.; Tomasi, J.; Barone, V.; Mennucci, B.; Cossi, M.; Scalmani, G.; Rega, N.; Petersson, G. A.; Nakatsuji, H.; Hada, M.; Ehara, M.; Toyota, K.; Fukuda, R.; Hasegawa, J.; Ishida, M.; Nakajima, T.; Honda, Y.; Kitao, O.; Nakai, H.; Klene, M.; Li, X.; Knox, J. E.; Hratchian, H. P.; Cross, J. B.; Bakken, V.; Adamo, C.; Jaramillo, J.; Gomperts, R.; Stratmann, R. E.; Yazyev, O.; Austin, A. J.; Cammi, R.; Pomelli, C.; Ochterski, J. W.; Ayala, P. Y.; Morokuma, K.; Voth, G. A.; Salvador, P.; Dannenberg, J. J.; Zakrzewski, V. G.; Dapprich, S.; Daniels, A. D.; Strain, M. C.; Farkas, O.; Malick, D. K.; Rabuck, A. D.; Raghavachari, K.; Foresman, J. B.; Ortiz, J. V.; Cui, Q.; Baboul, A. G.; Clifford, S.; Cioslowski, J.; Stefanov, B. B.; Liu, G.; Liashenko, A.; Piskorz, P.; Komaromi, I.; Martin, R. L.; Fox, D. J.; Keith, T.; Al-Laham, M. A.; Peng, C. Y.; Nanayakkara, A.; Challacombe, M.; Gill, P. M. W.; Johnson, B.; Chen, W.; Wong, M. W.; Gonzalez, C.; Pople, J. A. *Gaussian 03*, revision B.01; Gaussian, Inc.: Wallingford, CT, 2004.
- (35) Hehre, W. J.; Radom, L.; Schleyer, P. v. R.; Pople, J. A. *Ab Initio Molecular Theory*; John Wiley & Sons: New York, 1986.
- (36) Roothaan, C. C. J. *Rev. Mod. Phys.* **1951**, *23*, 69.
- (37) Ditchfie, R.; Hehre, W. J.; Pople, J. A. *J. Chem. Phys.* **1971**, *54*, 724.
- (38) Hehre, W. J.; Ditchfie, R.; Pople, J. A. *J. Chem. Phys.* **1972**, *56*, 2257.
- (39) Hariharan, P. C.; Pople, J. A. *Theor. Chim. Acta* **1973**, *28*, 213.
- (40) Becke, A. D. *J. Chem. Phys.* **1996**, *104*, 1040.
- (41) Lee, C.; Yang, W.; Parr, R. G. *Phys. Rev. B* **1988**, *37*, 785.
- (42) Miertus, S.; Scrocco, E.; Tomasi, J. *Chem. Phys.* **1981**, *55*, 117.
- (43) Iwaoka, M.; Okada, M.; Tomoda, S. *J. Mol. Struct. (THEOCHEM)* **2002**, *586*, 111.
- (44) *Jaguar 5.5*; Schroedinger, LLC: Portland, OR, 2003.
- (45) Bachs, M.; Luque, F. J.; Orozco, M. *J. Comput. Chem.* **1994**, *15*, 446.
- (46) Rashin, A. A.; Young, L.; Topol, I. A. *Biophys. Chem.* **1994**, *51*, 359.
- (47) Corcelli, S. A.; Kress, J. D.; Pratt, L. R.; Tawa, G. J. *Pacific Symposium on Biocomputing '96*; World Scientific: River Edge, NJ, 1995; p 143.
- (48) Topol, I. A.; Tawa, G. J.; Caldwell, R. A.; Eissenstat, M. A.; Burt, S. K. *J. Phys. Chem. A* **2000**, *104*, 9619.
- (49) Gould, R. O.; Gray, A. M.; Taylor, P.; Walkinshaw, M. D. *J. Am. Chem. Soc.* **1985**, *107*, 5921.
- (50) Görbitz, C. H.; Dalhus, B. *Acta Crystallogr.* **1996**, *C52*, 1754.
- (51) Anitha, K.; Athimoolam, S.; Rajaram, R. K. *Acta Crystallogr.* **2005**, *E61*, o1604.
- (52) Śliwickowska, J.; Lipkowski, J. *Acta Crystallogr.* **2001**, *C57*, 187.
- (53) Bombicz, P.; Dittrich, B.; Strumpel, M.; Nabein, H.; Luger, P. *Acta Crystallogr.* **2000**, *C56*, 1447.
- (54) Perczel, A.; Csizmadia, I. G. *Int. Rev. Phys. Chem.* **1995**, *14*, 127.
- (55) Perczel, A.; Angyán, J. G.; Kajtár, M.; Viviani, W.; Rivail, J.-L.; Marcoccia, J.-F.; Csizmadia, I. G. *J. Am. Chem. Soc.* **1991**, *113*, 6256.
- (56) McAllister, M. A.; Perczel, A.; Csaszar, P.; Viviani, W.; Rivail, J.-L.; Csizmadia, I. G. *J. Mol. Struct. (THEOCHEM)* **1993**, *288*, 161.
- (57) Sahai, M. A.; Fejer, S. N.; Viskolcz, B.; Pai, E. F.; Csizmadia, I. G. *J. Phys. Chem. A* **2006**, *110*, 11527.
- (58) Chass, G. A.; Lovas, S.; Murphy, R. F.; Csizmadia, I. G. *Eur. Phys. J. D* **2002**, *20*, 481.
- (59) Bombasaro, J. A.; Rodríguez, A. M.; Enriz, R. D. *J. Mol. Struct. (THEOCHEM)* **2005**, *724*, 173.
- (60) Tomasi, J.; Persico, M. *Chem. Rev.* **1994**, *94*, 2027.
- (61) Rivail, J. L.; Rinaldi, D. Liquid state quantum chemistry. In *Computational chemistry: review of current trends*; Leszczynski, J., Ed.; World Scientific: Singapore, 1995.
- (62) Cramer, C. J.; Truhlar, D. G. Continuum solvation models. In *Solvent effects and chemical reactivity*; Tapia, O., Bertran, J., Eds.; Kluwer: Dordrecht, 1996.
- (63) Orozco, M.; Alhambra, C.; Barril, X.; Lopez, J. M.; Busquets, M. A.; Luque, F. J. *J. Mol. Model.* **1996**, *2*, 1.
- (64) Dillet, V.; Rinaldi, D.; Rivail, J. L. *J. Phys. Chem.* **1994**, *98*, 5034.
- (65) Dillet, V.; Rinaldi, D.; Bertran, J.; Rivail, J. L. *J. Chem. Phys.* **1996**, *104*, 9437.
- (66) Klamt, A.; Schüürmann, G. *J. Chem. Soc., Perkins Trans. 2* **1993**, *799*.
- (67) Andzelm, J.; Kölmel, C.; Klamt, A. *J. Chem. Phys.* **1995**, *103*, 9312.
- (68) Truong, T. N.; Stefanovich, E. V. *Chem. Phys. Lett.* **1995**, *240*, 253.
- (69) Mitra, S. N.; Subramanian, E. *Biopolymers* **1994**, *34*, 1139.
- (70) Maxfield, F. R.; Leach, S. J.; Stimson, E. R.; Powers, S. P.; Scheraga, H. A. *Biopolymers* **1979**, *18*, 2507.
- (71) Berman, H. M.; Westbrook, J.; Feng, Z.; Gilliland, G.; Bhat, T. N.; Weissig, H.; Shindyalov, I. N.; Bourne, P. E.: The Protein Data Bank. *Nucleic Acids Res.* **2000**, *28*, 235–242.